Continuum model description of thin-film growth morphology

Chung-Yu Mou*

Department of Physics, National Tsing-Hua University, Hsinchu, Taiwan 300, Republic of China

J. W. P. Hsu†

Department of Physics, University of Virginia, McCormick Road, Charlottesville, Virginia 22901

We examine the applicability of the continuum model to describe the surface morphology of a heterogrowth system: compositionally-graded, relaxed GeSi films on (001) Si substrates. Surface roughness versus lateral dimension was analyzed for samples that were grown under different conditions. We find that all samples belong to the same growth class, in which the surface roughness scales linearly with lateral size at small scales and appears to saturate at large scales. For length scales ranging from 1 nm to 100 μm, the scaling behavior can be described by a linear continuum model consisting of a surface diffusion term and a Laplacian term. However, in-depth analysis of nonuniversal amplitudes indicates the breaking of up-down symmetry, suggesting the presence of nonlinear terms in the microscopic model. We argue that the leading nonlinear term has the form of $\lambda_1(\nabla h)^2$, but its effect on scaling exponents will not be evident for length scales less than 1 mm. Therefore, the growth dynamics of this system is described by the Kuramoto-Sivashinsky equation, consisting of the two linear terms plus $\lambda_1(\nabla h)^2$, driven by Gaussian noise. We also discuss the negative coefficient in the Laplacian term as an instability mechanism responsible for large-scale film morphology on the final surface. [S1063-651X(97)05008-3]

PACS number(s): 05.40.+j, 82.20.Mj, 68.55.Jk, 07.79.Lh

I. INTRODUCTION

The dynamics of film growth has proven to be a rich and interesting phenomenon[1]. In an ideal homogrowth, during which the deposition rate is sufficiently low and the temperature of the substrate is high enough, the adatoms have enough time to find their optimal positions so that most adatoms are registered and the growing front has only small fluctuations around the equilibrium shape. The resulting film under this growth condition is smooth. Such quality of the film can be maintained indefinitely only if the atoms below the growing front are always kept in true equilibrium. In reality, however, growth usually happens in nonequilibrium conditions. In fact, the real power of thin-film growth is the capability to create new materials and to obtain desired physical properties via nonequilibrium growth. In practical applications, an often encountered situation is to have the thin film and the substrate be different materials, i.e., heterogrowth. In heterogrowth, the growth mode is usually not layer by layer [2]; instead, it depends on equilibrium material properties as well as kinetic parameters during growth. In the extreme case, it was demonstrated recently that the coherent strain in the film can be utilized to fabricate novel nanostructures [3].

During the last decade, much work has been devoted to understanding nonequilibrium film growth. There are several important features observed in the final surface morphology. First, surfaces are highly irregular. It is therefore impractical to predict or describe such surfaces in microscopic detail. A coarse-grained, statistical modeling is more appropriate. Secondly, certain large-scale features can survive in the final surface morphology. These features are manifestations of underlying microscopic instabilities. Thirdly, it is found, in numerous experiments and computer simulations, that analysis of the surface roughness versus the sample's linear dimensions provides a useful classification of growth mechanism [1,4]. Specifically, many surfaces exhibit self-affinity in which a scaling phenomenon is found:

$$\sigma(t) \equiv \sqrt{\langle[H(\mathbf{r},t)-\langle H(\mathbf{r},t)\rangle]^2\rangle} \sim A_\sigma L^\chi f[L/\xi(t)]. \quad (1)$$

Here the sample dimension is $L \times L$, $\sigma(t)$ is the surface roughness, $H(\mathbf{r},t)$ is the height of the surface at position $\mathbf{r}$ and time t, and $\langle H(\mathbf{r},t)\rangle$ is the average height. The length $\xi(t)$ denotes the characteristic length of the surface. If no other important length scale is present, $\xi(t)$ is the correlation length built up during the course of film growth and scales as $\xi(t) \sim (\widetilde{\nu} t)^{1/z}$. The exponents χ and z are useful in characterizing the surface morphology. Different growth mechanisms result in different exponents, while the details of growth manifest themselves only through nonuniversal amplitudes A_σ and $\widetilde{\nu}$. Along with the discovery of the above scaling phenomenon, much theoretical work has been devoted to constructing appropriate continuum models for describing the film growth. The goal is to reproduce these scaling results.

Experimentally, until now, most work has concentrated on the measurement of the exponents, which leaves open many important issues. For example, in previous work, no differentiation in material nature between film and substrate and no examination of the applicability of continuum models to surfaces with large features were ever carefully made. Many results are thus *a priori* only applicable to homogrowth systems and to growth without instability. Results

*Electronic address: mou@phys.nthu.edu.tw

†Electronic address: jhsu@virginia.edu

from model systems [4] show that the quantitative scaling characteristics of surface roughness depend on the particular material system; for example, the data for χ range from 0.2 to 1. It is therefore particularly important to examine the applicability of theoretical ideas, such as continuum modeling, beyond the homogrowth system.

In this paper, we examine a heterogrowth system: compositionally graded, relaxed GeSi films on (001) Si substrates. A distinct feature of surfaces in this system is the existence of large-scale patterns, known as cross hatches [5]. These patterns are closely related to the underlying misfit dislocation network. Much work has been devoted to understanding the mechanism responsible for the cross-hatch formation [6,7]. Here we approach this problem differently by examining how surface roughness depends on lateral size, i.e., by scaling analyses. In addition, we go beyond the usual approach, which is based solely on the measurement of roughness exponents, and perform more comprehensive analyses on nonuniversal amplitudes and the up-down symmetry of surfaces. Our results indicate that, up to a length scale of 100 μm, a continuum model in which the linear parts are composed of a surface diffusion term and a Laplacian term is appropriate for describing these surfaces. The breaking of up-down symmetry shows that nonlinearities must also be present. Detailed analysis sets a lower bound of ≈ 1 mm for observing the scaling exponents that arise from the lowest-order nonlinear term. The resulting continuum model that is consistent with the experimental data is a two-dimensional Kuramoto-Sivashinsky equation driven by Gaussian noise [8]. We also discuss the instability that might be responsible for the cross-hatch formation in the framework of a continuum description.

This paper is organized as follows. Section II briefly reviews relevant theoretical ideas and results. In Sec. III, we apply scaling analyses to study the surface morphology of relaxed GeSi films grown on Si substrates. Both universal scaling exponents and non-universal amplitudes are analyzed. The restrictions placed on the proposed continuum model by the experimental results and the crossover from this model to other models are discussed in Sec. IV. The Appendices are devoted to more technical details. In Appendix A, we calculate the surface roughness for a sinusoidal surface. In Appendix B, we apply the Dyson-Wyld renormalized perturbation theory to analyze one of the possible growth models that can account for our results.

II. CONTINUUM MODELS AND THEORETICAL RESULTS

We begin with a brief review of the theoretical situations. There are two useful asymptotic behaviors for $f(y)$ in Eq. (1). When $L \ll \xi(t)$, the whole sample evolves ''coherently'' in the sense that $\sigma(t)$ is independent of time; hence $f(y) \sim 1$ as $y \rightarrow 0$. This implies that, in the limit of large t $[L \ll \xi(t)]$, $\sigma \sim A_\sigma L^\chi$. At the opposite limit, when $L \gg \xi(t)$, the local surface roughness has not detected the existence of the boundary of the sample, so $\sigma(t)$ does not depend on L. One then deduces that $f(y) \sim y^{-\chi}$ as $y \rightarrow \infty$ [9]. That is, in the limit of small t, $\sigma \sim A_\sigma (\widetilde{\nu} t)^\beta \equiv A_t t^\beta$, with $\beta = \chi/z$.

In order to explain the above scaling phenomena and calculate the relevant exponents, a number of continuum models have been proposed [10–13]. In these models, $H(\mathbf{r}, t)$ is

coarse grained. The interface growth is modeled by noise-driven dynamics:

$$\frac{\partial h}{\partial t} = \mathrm{F}[h] + \eta(\mathbf{r}, t). \qquad (2)$$

Here $h = H - \langle H \rangle$, $\langle H \rangle$ being the average height and $\eta(\mathbf{r}, t)$, representing fluctuations in the deposition flux, is modeled by Gaussian white noise with the two-point correlation function given by

$$\langle \eta(\mathbf{r_1}, t_1) \eta(\mathbf{r_2}, t_2) \rangle = 2\eta_0 \delta(\mathbf{r_1} - \mathbf{r_2}) \delta(t_1 - t_2). \qquad (3)$$

The rest of the growth dynamics is lumped into $\mathrm{F}[h]$ in which different driving forces for adatom movement are represented by different terms. A characteristic of these models is that the resulting surfaces are usually driven towards being self-affine, resulting in the above scaling behaviors.

The continuum models can be classified into two classes: conservative and nonconservative. In nonconservative dynamics, the flow of atoms onto the surface is assumed to be normal to the surface. The Kardar-Parisi-Zhang (KPZ) model, in which $F[h] = \nu \nabla^2 h + \lambda_1 (\nabla h)^2$ with $\nu > 0$, represents the lowest-order realization of such dynamics. Here $\lambda_1 (\nabla h)^2$ accounts for the fact that the growth is normal to the interface, and the desorption, accounted for by $\nu \nabla^2 h$, is assumed to be important [12,13]. The exponents of this model for dimensionality (d) of $1+1$ are known exactly: $\chi = 1/2$ and $z = 3/2$, while only numerical results are available for $d = 2+1$ [14].

In conservative dynamics, one only includes the flow of atoms parallel to the surface. Therefore, $F[h]$ must take the form

$$F[h] = -\boldsymbol{\nabla} \cdot \mathbf{J},$$

where $\mathbf{J}$ is the surface adatom current and the total volume $\iint dx dy h(x, y)$ is conserved. It has been argued that conservative dynamics is the main scenario that occurs in the molecular beam epitaxy (MBE) growth. In particular, surface diffusion, rather than desorption, is the dominating factor [10–12]. The surface diffusion is assumed to be driven by the energetics of adatoms on surfaces so that $\mathbf{J}$ obeys the Fick's law $\mathbf{J} = -\alpha \nabla \mu$, where μ is the chemical potential on surfaces. A couple of mechanisms contributing to μ have been proposed. First, because adatoms have fewer (more) bonding opportunities when they reside on ''mountains'' (''valleys''), μ is proportional to the curvature [15]. Secondly, adatoms on slopes either have higher kinetic energy or their chemical bonds are more stretched. One thus expects that they have higher μ. This effect may be accounted for by the term $(\nabla h)^2$ [11]. Combining these two mechanisms, Lai and Das Sarma (LS) investigated the model in which $F[h] = -K \nabla^4 h + \lambda_2 \nabla^2 (\nabla h)^2$ [11]. Here $-K \nabla^4 h$ is the lowest-order contribution from the curvature. They found the exponents to be $\chi = 2/3$ and $z = 10/3$ for $d = 2+1$.

The existence of a Laplacian term is an important question, for in order to see the exponents predicted by the LS model, there must be *no Laplacian term*. A nonvanishing Laplacian term, no matter how small, will make λ_2 irrelevant, resulting in different scaling exponents from the LS results [16]. There are several mechanisms that can generate

TABLE I. Detailed growth parameters (R_1 and R_2 are the growth and grading rates) and nonuniversal amplitudes obtained from our analysis of samples $A-E$: σ_0 and θ_0 are saturated values of surface roughness and $|\langle h^3 \rangle|^{1/3}$, respectively.

Sample	A	B	C	D	E
Ge(%)	30	30	30	40	30
Growth method	MBE	MBE	MBE	CVD	CVD
T (°C)	900	900	900	850	650
P (mT)				2	50
R_1 (Å / sec)	3	3	3	7	12
R_2 (Ge%/μm)	10	80	80	10	10
L_ν (μm)	1.5	0.67	1.05	2.0	5.5
σ_0 (Å)	37 ± 4	65 ± 4	186 ± 15	61 ± 7	124 ± 5
θ_0 (Å)	13 ± 4	19 ± 5	91 ± 38	29 ± 11	51 ± 6
$A_\sigma^{(\nu)}$ (Å)	12	22	65	20	38
$A_\sigma^{(K)}$ (10^{-4})	26	87	169	29	28
$A_\sigma^{(\nu)}\sqrt{\ln(L_\nu/a)}$ (Å)	34	58	178	57	115

Laplacian terms. The typical way to generate the Laplacian term is via the desorption, which is small but is not identically zero [1]. If surfaces are liquidlike, a Laplacian term can arise from nonvanishing surface tension. More recently, Villain [12] argued that the combination of surface diffusion on terraces and step-edge (Schwoebel) barriers results in a Laplacian term. The coefficient ν of the Laplacian term, however, is negative when growing on singular (i.e., high-symmetry) surfaces.

Theoretically, a negative ν leads to unstable surface growth, producing large-scale features on surfaces. This phenomenon was observed in a recent Monte Carlo study [17]. For continuum models, when the negative Laplacian term is combined with the surface diffusion term $-K\nabla^4 h$ and the KPZ nonlinear term, the resulting dynamics (without noise), known as the Kuramoto-Sivashinsky (KS) equation, is particularly interesting [8]. The KS equation has been used to describe a wide class of phenomena associated with instabilities such as flame propagation and chemical turbulence. It is linearly unstable, but is nonlinearly chaotic, exhibiting spatiotemporal chaos. Many years ago, Yakhot [18] conjectured that the nonlinear term in the KS equation (with random initial conditions) will ''renormalize'' the negative ν so that the effective large-scale behavior of the KS equation can be described by the KPZ equation with a positive, effective ν. In one dimension, this is confirmed by a recent work of Chow and Hwa [19]. In two dimensions, however, conflicting results have been reported [20,21]. There appears to be no consensus about the scaling behavior of the KS equation at large scales, though they all agree that an effective, positive ν must be present at large length scales. Experimentally, quantitative evidence of a nonvanishing Laplacian term was not established until recently [22], although an earlier study used a negative ν to explain the large-scale features in homogrowth of GaAs films [17].

A negative ν is not the only possible mechanism for generating large features on surfaces, i.e., rough surfaces. In fact, it has been recognized that a flat surface under stress may become unstable or metastable [23]. Several stress-induced instability mechanisms have been proposed. In the continuum elastic theory [24], an elastic energy is added to the chemical potential, resulting in a linear term, $ck^3 h(\mathbf{k},t)$, in Fourier space. Here c is a positive constant. Tersoff et al. have proposed a long-range attractive interaction between steps on vicinal strained layers [23]. The interaction leads to step-bunching instability and, effectively, it also introduces the term $k^3 h(\mathbf{k},t)$ but with a different coefficient c'. It is important to note that these theories were derived for strained films without dislocations. The k^3 term is nonlocal and not analytic in real space, and thus is absent in the gradient expansion of $F[h]$.

III. EXPERIMENTS AND RESULTS

GeSi films studied here were grown either by MBE or by low pressure chemical vapor deposition (CVD) [25]. In order to minimize threading dislocation density, the Ge concentrations in these films were increased linearly with the average film thickness until desired compositions were achieved. The growth temperature for these samples was sufficiently high so as to achieve strain relaxation during growth [6]. The average lattice constants of the films are the same as those of bulk crystals, i.e., completely relaxed. Detailed characterization of these samples is given in Refs. [6] and [26]. We concentrate on samples with approximately the same final Ge composition but grown under different conditions. We also examine samples grown with different grading rates. Relevant growth information and nonuniversal amplitudes obtained from our analysis for five samples are summarized in Table I.

The surface roughness was measured using a scanning force microscope (SFM). Large-scale (48 μm)^2 SFM images of all five samples are shown in Figs. 1(a)–1(e). All samples except sample C display a long-range ordered cross-hatch pattern on the surface [27]. We shall see that the ordering of the cross-hatch pattern does not affect the scaling behavior of the surface roughness. In Figs. 2(a) and 2(b), we show samples B and C respectively, on a magnified scale, (14.5 μm)^2. The line cuts (height changes versus lateral distances) indicated in Figs. 2(a) and 2(b) are shown in Figs. 2(c) and 2(d), respectively. To determine the surface roughness at length scales varying from 1 nm to 100 μm, images (256
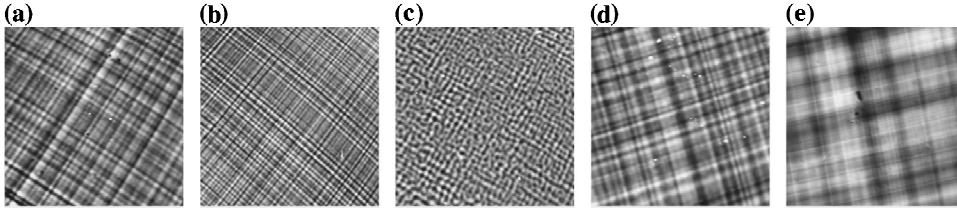
FIG. 1. SFM images of samples listed in Table I: A (a), B (b), C (c), D (c), and E (d), respectively. The image sizes are $(48 \ \mu\text{m}) \times (48 \ \mu\text{m})$.

pixel $\times$ 256 pixel) similar to Figs. 1(a)–1(e) were taken at different length scales and on at least two random spots for a given sample. When performing scaling analysis, we divided each image into smaller images (128×128, $64 \times 64, \ldots, 2 \times 2$). The roughness for a given length scale L was obtained by first calculating the rms roughness inside each $L \times L$ image, then averaging over the ensemble of images of the same size [28]. To obtain data for L from 1 nm to 100 μm, we combine results from several images of different sizes.

Figure 3(a) shows σ versus L in a log-log plot for all five samples. These curves all show similar behaviors, i.e., $\sigma \propto L^1$ at small length scales over *3 decades* in both σ and L, and σ flattens out with zero slopes ($\chi \sim 0$) above some sample-dependent crossover length $L_\nu = 0.5 \sim 10 \ \mu$m. At larger length scales, all surfaces are flat in the sense that the surface roughness reaches a saturated value (σ_0) that is almost independent of the system size. For the five samples we studied, σ_0 ranges from 37 to 186 Å, and L_ν from 0.7 to 5.5 μm (see Table 1). These differences are more easily seen in Figs. 2(a)–2(d), especially the difference for σ_0 [Figs. 2(c) and 2(d)]. Note that the y axis (height change) in Fig. 2(d) is twice that in Fig. 2(c). When we rescale L by L_ν and σ by σ_0, all the data collapse onto one universal curve, as shown in Fig. 3(b). The successful collapsing demonstrates that, despite the differences in synthesis parameters and apparent surface morphology, all samples belong to the same growth universality class governed by $\sigma/\sigma_0 = f(L/L_\nu)$, where the collapsed data points in Fig. 3(b) trace out the universal scaling function f. The collapsing of data indicates that all samples can be described by the same continuum model, if

there exists an appropriate one. It also implies that the order of the cross-hatch pattern is not relevant since the surface of sample C does not display the ordered the cross-hatch pattern but can still be collapsed with the other data.

A simple power counting suggests that scaling results shown in Fig. 3 can be accounted by the linear model:

$$F[h,t] = \nu \nabla^2 h - K \nabla^4 h. \tag{4}$$

Since the $-K\nabla^4 h$ term represents surface diffusion [12,29], which tends to stabilize growth, K is taken to be positive. In this model ($d = 2+1$), when $-K\nabla^4 h$ dominates, $\chi = 1$; while if $\nu\nabla^2 h$ dominates, $\chi = 0$ [1]. The crossover length L_ν between the two scaling regimes is set by $2\pi(K/|\nu|)^{1/2}$. The good agreement in scaling exponents between experi-
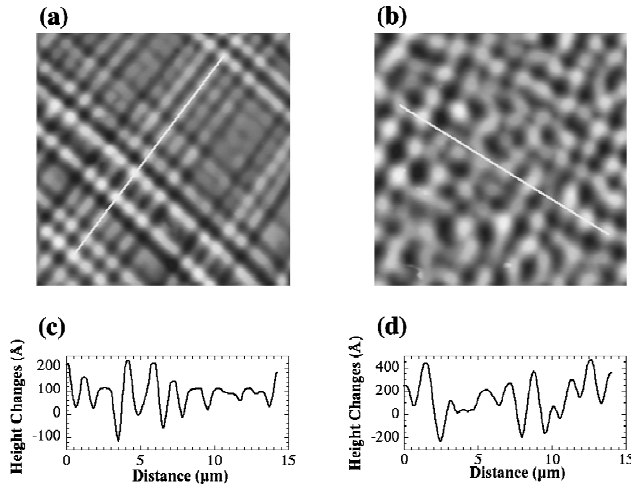
FIG. 2. $(14.5 \ \mu\text{m}) \times (14.5 \ \mu\text{m})$ SFM images of samples B (a) and C (b), respectively. The surface roughness line cuts (height change vs lateral distance) indicated by the white lines in (a) and (b) are shown in (c) and (d), respectively.
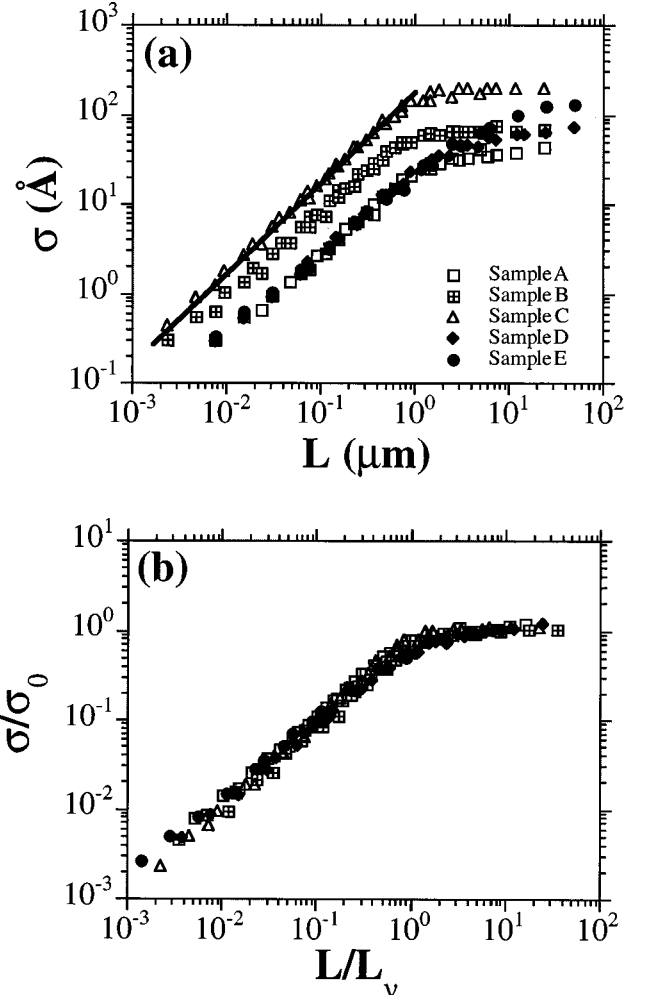
FIG. 3. (a) Surface roughness (σ) vs L for all 5 samples in Table I. The calculation of $\sigma(L)$ is given in the text. The line represents $\sigma \propto L^1$. (b) σ/σ_0 vs L/L_ν for all samples.
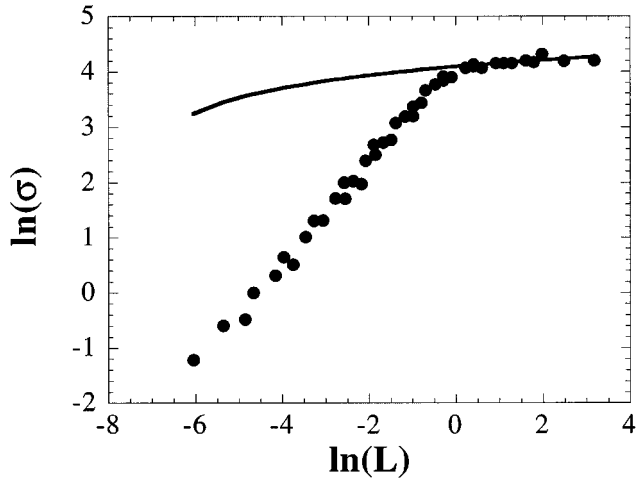
FIG. 4. A logarithmic fit to the data of sample B. The lattice constant obtained from this fit is about 6 Å, and $A_\sigma^{(\nu)} = \sqrt{\eta_0/(2\pi|\nu|)}$ is 22 Å.

mental results and the model shows that surface diffusion dominates at small length scales.

In a more detailed analysis, we introduce an infrared cutoff $k_0 (\equiv 2\pi/L)$ and an ultraviolet cutoff Λ ($\equiv 2\pi/a$, where a is the lattice constant) [30] so that the roughness can be calculated via the integral

$$\sigma(L) = \int_{k_0}^{\Lambda} \frac{d^2\mathbf{k}}{(2\pi)^2} \int d\omega \langle h(\mathbf{k},\boldsymbol{\omega}) h(-\mathbf{k},-\boldsymbol{\omega}) \rangle. \quad (5)$$

When $\nu\nabla^2 h$ dominates, we find $\sigma_\nu \sim \sqrt{\eta_0/(2\pi|\nu|)}\sqrt{\ln(L/a)}$. In Fig. 4, we show our fit for sample B. The lattice constant read off from this fitting is about 6 Å, which is comparable to the lattice constant of $Ge_{0.3}Si_{0.7}$. Similar fittings have also been done for the other samples, and they are all consistent with this form. In this regime, the nonuniversal amplitude $A_\sigma^{(\nu)}$ is $\sqrt{\eta_0/(2\pi|\nu|)}$. The experimentally observed values for $A_\sigma^{(\nu)}$ range from 12 to 65 Å (see Table I). The saturation roughness σ_0 is related to $A_\sigma^{(\nu)}$ via the relation $\sigma_0 = A_\sigma^{(\nu)}\sqrt{\ln(L_0/a)}$, where L_0 is the scan size in the Laplacian term dominant region. Since for all samples $\sqrt{\ln(L_0/a)}$ is about 3, σ_0 and $A_\sigma^{(\nu)}$ are of the same order. Using L_ν, determined from the crossover of the scaling exponents, and $A_\sigma^{(\nu)}$, determined from a logarithmic fit of the saturation region, to calculate $A_\sigma^{(\nu)}\sqrt{\ln(L_\nu/a)}$, the results agree very well with experimentally measured σ_0 for all five samples (see Table I). The reason $A_\sigma^{(\nu)}\sqrt{\ln(L_\nu/a)}$ is consistently smaller than σ_0 comes from the fact that $L_\nu < L_0$. At small length scales ($L < L_\nu$), if $-K\nabla^4 h$ dominates, we get $\sigma_K \sim \sqrt{\eta_0/(16\pi^3 K)}L$. Here $A_\sigma^{(K)}$ is $\sqrt{\eta_0/(16\pi^3 K)}$, which is the slope $d\sigma/dL$ for $L < L_\nu$. Experimentally, we can independently determine 3 parameters: σ_0, $A_\sigma^{(K)}$, and L_ν. For our data to be consistent with Eq. (4), these parameters must satisfy $\sigma_0/A_\sigma^{(K)} \approx 4.75 L_\nu$. In Fig. 5, we plot $\sigma_0/A_\sigma^{(K)}$ versus L_ν. We see that the linearity between $\sigma_0/A_\sigma^{(K)}$ and L_ν is quite good, though the slope is 1 and not 4.75. This shows that as far as scaling is concerned, the above linear model describes the growth of this real, complex heterogrowth system reasonably well.
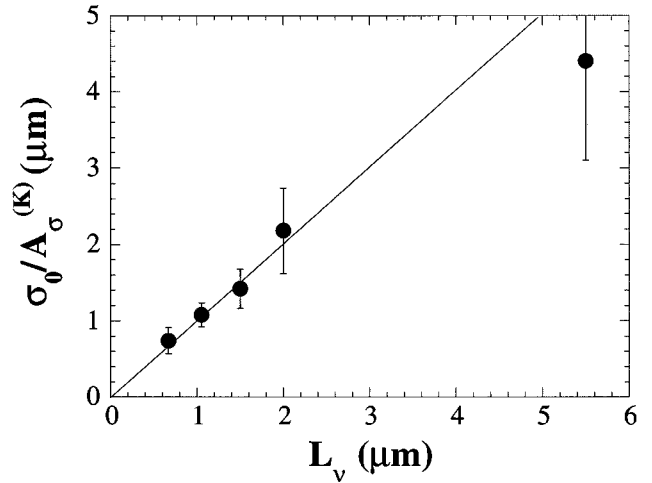
FIG. 5. Ratio of nonuniversal amplitudes $\sigma_0/A_\sigma^{(K)}$ vs the crossover length L_ν. The line is a guide to the eye with slope $= 1$.

The discrepancy between the measured slope for $\sigma_0/A_\sigma^{(K)}$ versus L_ν and the predicted value from scaling suggests that nonlinear terms do not identically vanish. Therefore, as a test of linearity, we also examine the value of $\theta \equiv |\langle h^3 \rangle|^{1/3}$. In all samples, we found nonzero θ's (see Table I). There is no apparent enhancement of θ from increasing the grading rate (samples B and C). In Fig. 6, we show the plot of θ versus L for sample B. Even though the data are more noisy, it shows that θ has a similar dependence on L to that of the roughness. This indicates that these surfaces are not multiaffine [1]. The nonvanishing of θ implies that the up-down symmetry is broken and thus a nonlinear term must be present. The lowest-order nonlinear term appears to have no effect on the scaling behavior of σ below 100 μm (including the linear relation between $\sigma_0/A_\sigma^{(K)}$ and L_ν), but they are important in determining factors besides scalings such as the slope between $\sigma_0/A_\sigma^{(K)}$ and L_ν.

We can further estimate the magnitudes of ν, K, and η_0. Assuming that surface diffusion is induced by variations of the chemical potential, K is given by $D_s\gamma\Omega^2 n/k_B T$ [29], where D_s is the surface diffusion constant, n is the areal density of adatoms [12], γ is the surface tension, and Ω is atomic volume. At relevant growth temperatures, D_s is of
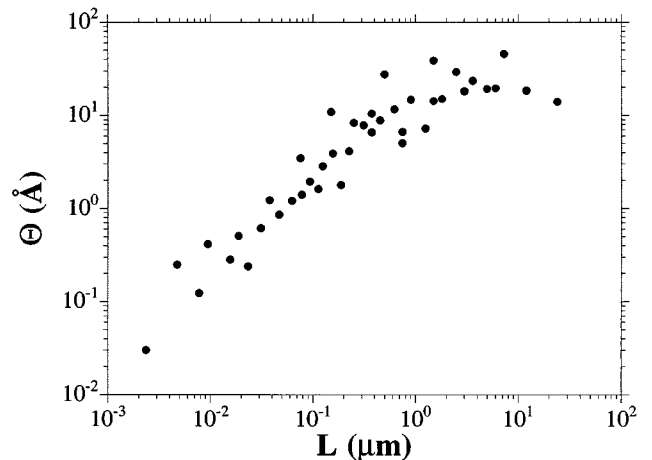
FIG. 6. The third moment $\theta \equiv |\langle h^3 \rangle|^{1/3}$ vs L for sample B.

order 10^{-5} cm^2/sec [31], while $\gamma \sim 10^3$ erg/cm^2 [2]. The values of the remaining parameters are standard [32]. Altogether, we find that $K \sim 10^{-20}$ cm^4 sec^{-1}, which implies that $|\nu|$ is of order 10^{-2} μm^2 sec^{-1} via $2\pi(K/|\nu|)^{1/2} \sim L_\nu \sim 1$ μm. From the relation $A_\sigma^{(\nu)} \sim \sqrt{\eta_0/(2\pi|\nu|)}$ and the experimental values of $A_\sigma^{(\nu)}$ and $|\nu|$, we find $\eta_0 \sim 10^{-23}$ cm^4/sec.

Another important feature in Fig. 3 is that samples with faster grading rate (80% Ge/μm), such as samples B and C, are rougher (with larger σ and $A_\sigma^{(K)}$) for $L < L_\nu$. In addition, σ for samples A, D, and E, all of which were grown at 10% Ge/μm grading rate, are identical at small length scales. For a relaxed film, strain fields are not uniform in the films, but concentrate near dislocations [6]. The larger grading rate means that the growth surface is closer to the dislocations and therefore the surface strain fields are larger. Hence, the larger $A_\sigma^{(K)}$'s observed in the 80% Ge/μm grading rate samples suggest that strain enhances surface roughness. From a different point of view, since the primary effect of the $-K\nabla^4 h$ term is to decrease roughness, our results indicate that strain fields suppress adatom diffusion on the surface.

IV. DISCUSSION AND CONCLUSIONS

We now examine our results more closely. First, the relation $A_\sigma^{(\nu)}/A_\sigma^{(K)} \approx L_\nu$ has a natural geometrical meaning. It reflects the wavy nature of the surface morphology in our samples: if one treats $A_\sigma^{(\nu)}$ approximately as the amplitude of the wave, $A_\sigma^{(K)}$ as the slope from the valley to the peak, and L_ν as the width from peak to peak, the relation $A_\sigma^{(\nu)}/A_\sigma^{(K)} \approx L_\nu$ follows from the definition of slope. In Appendix A, we calculate the surface roughness of a continuum sinusoidal surface. The surface roughness of this model surface has a similar saturation for $L \gg L_\nu$, but in the opposite limit $L \ll L_\nu$ the roughness does not have an exact linear scaling relation with L. One should be further cautious that the real surface is not exactly a sinusoidal wave. In Figs. 2(c) and 2(d), we show the surface roughness line cuts for samples B and C, respectively. The local slopes vary from <10 Å/μm to >800 Å/μm for sample B and >1000 Å/μm for sample C, indicating that these surfaces contain more than one wavelength.

Secondly, the experimentally observed ν ($\equiv \nu_E$) is an effective one and must be positive. If ν is negative, $h(\mathbf{k},t)$ grows exponentially. The roughness would not saturate at large times. In this case, one finds the roughness $\sigma(t,L)$ by expressing the height in terms of η:

$$h(\mathbf{k},t) = \int_0^t dt' \exp(|\nu| k^2 t') \eta(\mathbf{k},t'),$$

and calculates the correlation function $\langle h(\mathbf{k},t) h(\mathbf{k}',t) \rangle$. The roughness is then determined by the integral $\int d^2\mathbf{k} \int d^2\mathbf{k}' \langle h(\mathbf{k},t) h(\mathbf{k}',t) \rangle$. We obtain

$$\sigma^2(L,t) = \frac{\eta_0}{2\pi|\nu|}\left[\int_{2\pi/L}^{2\pi/a} \frac{\exp(2|\nu|k^2 t)}{k} dk - \ln\frac{L}{a} \right]$$

$$= \frac{\eta_0}{4\pi|\nu|}\left[\mathrm{Ei}\left(8|\nu|\pi^2 \frac{t}{a^2} \right) - \mathrm{Ei}\left(8|\nu|\pi^2 \frac{t}{L^2} \right) - 2\ln\frac{L}{a} \right], \tag{6}$$

where Ei is the exponential integral function and we have assumed that initially the surface is flat, i.e., $\sigma^2(L,0) = 0$. For our samples, the growth time is about 10^4 sec and $\Lambda \simeq 1$ Å$^{-1} \approx 10^4(2\pi/L)$, so the order of $2|\nu_E|\Lambda^2 t$ is 10^{10}, which is very large. As a result, the first term dominates so that $\sigma(L,t)$ is approximately independent of L. Therefore, if ν_E is negative, its value, when combined with Eq. (6) and the observed σ_0, yields a value of η_0 at the order of 10^{-10^9} cm^4 sec^{-1}, which is unreasonably small. It therefore implies that ν_E cannot be negative.

What is the bare growth equation that can generate the observed cross-hatch pattern and yet result in a positive ν_E at large length scales? At first, it seems that the term $ck^3 h(\mathbf{k},t)$, induced by the stress, must be present. However, as mentioned earlier, this term was derived only for strained films without dislocations, while our samples are completely relaxed. Therefore, we do not include it and consider the case when the bare ν ($\equiv \nu_0$) that appears in the growth equation is negative [12]. This coefficient ν_0 enters the roughness $\sigma(L,t)$ at very early times. When t is very small, because the height h of the surface is still small, the nonlinear terms, which are of higher order in h, can be neglected. Therefore, $F[h]$ in the growth equation can be simply approximated by a negative Laplacian term $\nu_0 \nabla^2 h$. Equation (6), with ν replaced by ν_0, then describes the roughness only when t is very small. The value of ν_0 may be obtained, for example, by measuring the first and second time derivatives of surface roughness via the relation

$$\frac{d^2}{dt^2}\sigma^2(L,t)\bigg|_{t=0} = |\nu_0|[\Lambda^2 + (2\pi/L)^2]\frac{d}{dt}\sigma^2(L,t)\bigg|_{t=0}, \tag{7}$$

where we have expressed η_0 in terms of the initial increase rate of $\sigma^2(L,t)$. After a short period of initial growth, the height h has grown so large that one cannot ignore the effects of nonlinearity any more. According to the standard picture of pattern formation [33], nonlinear terms then saturate the initial unstable growth, resulting in the final morphology. If ν_0 is negative due to Schwoebel barriers [12], we expect the growth on vicinal surfaces will be much smoother because the bare ν is positive even at early times. This is indeed observed experimentally [5].

There are a couple of important issues that need to be addressed: (1) What are the large-scale [34] scaling behaviors of the final morphology? (2) What are the nonlinear terms that enter the growth equation? From our results, it is clear that up to 100 μm, the scaling behaviors at large length scales are captured by the growth equation composed of a Laplacian term with an effective, *positive* ν. This fact also provides us with some insight about the leading-order nonlinear term. In Appendix B, we examine in detail the combined growth equation, $F[h,t] = \nu_0 \nabla^2 h - K\nabla^4 h$

$+\lambda_2\nabla^2(\nabla h)^2$, within the framework of Dyson-Wyld renormalized perturbation theory [20]. We show that ν_0 does not get any correction that comes from $\lambda_2\nabla^2(\nabla h)^2$ in the large length scale limit. This result reflects what we mentioned earlier: λ_2 is irrelevant in the presence of a Laplacian term. Thus, we are left with $\lambda_1(\nabla h)^2$ as the only possible leading nonlinear term. The resulting growth equation is the KS equation, driven by Gaussian noise. As discussed in Sec. II, the situation of theoretical work on the large length scale scaling behaviors of the KS equation [8,18,19] is not clear now. In fact, the reported results for the two-dimensional case are conflicting. Nevertheless, they all agree that an effective and positive ν must present at large length scales. This appears to be precisely what we observe. Although we are not able to resolve the theoretical conflict using these experimental results, detailed analyses of our results set a minimum size of the sample for resolving this conflict. Because we did not observe the scaling exponents predicted by the KPZ equation, if $\lambda_1(\nabla h)^2$ survives in the effective equation, its effect must be small for length scale below 100 μm. The lower end of this nonlinear term dominant regime must match with the upper end of the regime dominated by the Laplacian term. Since the characteristic time scale in the nonlinear regime is $\tilde{\nu}L^z$, matching the time scales in two regimes defines a crossover length L_c:

$$L_c \approx \left(\frac{\nu}{\tilde{\nu}}\right)^{1/(2-z)}, \qquad (8)$$

where z and $\tilde{\nu}$ are the corresponding exponent and nonuniversal amplitude in the KPZ regime. Another relation can be obtained by matching the roughness. We find that

$$A_\sigma \gtrsim \frac{A_\sigma^{(\nu)}\ln(L_c/a)}{L_c^\chi}, \qquad (9)$$

where A_σ and A_t (in the following equation) represent the corresponding nonuniversal amplitudes in the KPZ regime. Since $A_t = A_\sigma(\tilde{\nu})^\beta$, we obtain

$$L_c \gtrsim \sqrt{\nu[A_\sigma^{(\nu)}\ln(L_c/a)/A_t]^{z/\chi}}. \qquad (10)$$

Because we do not observe any crossover below 100 μm, L_c has to be larger than 100 μm. In addition, by setting L_c on the right-hand side of Eq. (10) to the maximal scan size L_0, we can get an estimate of the lower bound for L_c. Using the figures $z/\chi\approx 4$, $A_\sigma^{(\nu)}\ln(L_0/a)\approx 10^2$ Å for $L_0\approx 100$ μm, $A_t\sim 1$ Å/(sec)$^\beta$, and $\nu\approx 10^{-2}$ μm^2 sec^{-1}, we find that the lower bound is about 1 mm, which is beyond our measurement range.

In conclusion, we have observed a universal scaling behavior for the surface morphology of compositionally graded, relaxed GeSi/Si(001) films. Quantitative analyses on scaling exponents and nonuniversal amplitudes show that the scaling behaviors for samples grown under different conditions all belong to the same universality class, which can be described by the linear model $F[h,t]=\nu\nabla^2h - K\nabla^4h$ for 1 nm$\lesssim L \lesssim$ 100 μm. In combination with further theoretical analyses, it is argued that the underlying growth model is the KS equation driven by Gaussian noise. Our results indicate that as far as the roughening exponents are concerned, up to

100 μm, the effective theory of the KS equation is the linear model, pushing the length scale for observing the KPZ scaling exponents to be above 1 mm.

APPENDIX A

In this Appendix, we demonstrate some features of the surface roughness for a continuum wavy surface. Specifically, we shall consider a sinusoidal surface $y=y_0\sin(2\pi x/L_\nu)$, but many features do not depend on the particular form we choose. Since one only measures discrete points in experiments (the number of pixels determining the distance between adjacent points), we assume that $L_\nu = N_\nu\varepsilon$, where N_ν is a positive integer and ε is the distance between adjacent points. The experimental data then consist of $2N+1$ equidistant points (x_n, h_n) centered at (x_0, h_0), where we have defined $h_i = y_0\sin(2\pi x_i/L_\nu)$ and $x_n - x_0 = n\varepsilon$ with n ranging from $-N$ to N. The surface roughness can be found by evaluating the following sums:

$$\langle h\rangle = \frac{y_0}{2N+1}\sum_{n=-N}^{n=N}\sin\frac{2\pi(n\varepsilon+x_0)}{N_0\varepsilon}, \qquad (A1)$$

$$\langle h^2\rangle = \frac{y_0^2}{2N+1}\sum_{n=-N}^{n=N}\left[\sin\frac{2\pi(n\varepsilon+x_0)}{N_0\varepsilon}\right]^2. \qquad (A2)$$

For large N_ν, these sums become integrals. Evaluating these integrals, one obtains a surface roughness $\sigma(N,L_\nu,x_0)$, which depends on both x_0 and L_ν. If the modulation on the surface contains only one wavelength, the global surface roughness is simply an average of x_0 over the period L_ν. We find that

$$\sigma = y_0\left[\frac{L}{2L+\varepsilon} - \left(\frac{L_\nu}{2L+\varepsilon}\frac{1}{2\pi}\right)^2\left(1-\cos\frac{4\pi L}{L_\nu}\right)\right]^{1/2}, \qquad (A3)$$

where L $(=N\varepsilon)$ is the size of the sample. In this case, σ approaches y_0 as L approaches ∞. For $L<L_\nu$, σ does not scale; instead, it oscillates with L.

APPENDIX B

In this appendix, we shall investigate the large-scale behavior of the model

$$\frac{\partial h}{\partial t} = \nu_0\nabla^2h - K\nabla^4h + \lambda_2\nabla^2(\nabla h)^2 + \eta, \qquad (B1)$$

where ν_0 is *negative*. Specifically, we shall show that there is no correction to ν_0 at large length scales.

Two important functions we shall work with are the response function $G(k,\omega)$ and the two-point correlation function $U(k,\omega)$. They are defined by

$$G(k,\omega) \equiv \left\langle \frac{\delta h(\mathbf{k},\omega)}{\delta \eta(\mathbf{k},\omega)} \right\rangle_{\eta \to 0}, \qquad (B2)$$

$$U(k,\omega) \equiv \langle h(\mathbf{k},\omega) h(-\mathbf{k},-\omega) \rangle. \qquad (B3)$$

The generic forms of these functions are [20]

$$G(k,\omega) = \frac{1}{-i\omega + \gamma_k + \Sigma(k,\omega)}, \qquad (B4)$$

$$U(k,\omega) = |G(k,\omega)|^2 [2\eta_0 + \Phi(k,\omega)] \qquad (B5)$$

where $\gamma_k = -\nu_0 k^2 - K k^4$ and $\Sigma(k,\omega)$ and $\Phi(k,\omega)$ are the self-energies. We shall be interested in scaling solutions in which $G(k,\omega) = g(\omega/\nu k^z)/\nu k^z$ and $U(k,\omega) = u(\omega/\nu k^z)/k^\Delta$. These scaling solutions are asymptotically correct only for $k \to 0$ and $\omega \to 0$. Therefore, γ_k has to be subdominant to νk^z for $k \to 0$; hence $z \leq 2$. The exponents z and Δ are related to χ via the relation $2\chi = \Delta - d - z$. We shall show that $z = 2$ is not acceptable.

Let us first consider the one-loop diagrams in the renormalized Wyld-Dyson perturbation theory [20]. The self-energy is

$$\Sigma^{(2)}(k,\omega) = 4(\lambda_2)^2 \int_{\mathbf{q}} \int_\Omega [k^2 (\mathbf{k}-\mathbf{q}) \cdot \mathbf{q}]$$
$$\times [q^2 \mathbf{k} \cdot (\mathbf{k}-\mathbf{q})] G(q,\Omega) U(|\mathbf{k}-\mathbf{q}|, \omega - \Omega). \qquad (B6)$$

By appropriate changes of variables $\mathbf{Q} = \mathbf{q}/k$, $t = \Omega/\nu q^z$, and $s = \omega/\nu k^z$, we can rewrite Eq. (B6) in the following form:

$$\Sigma^{(2)}(k,\omega) = k^{d+8-\Delta} \sigma^{(2)}(s, \Lambda/k, m_0/k). \qquad (B7)$$

Here $\sigma^{(2)}$ is a function of s, Λ/k, and m_0/k. Λ and m_0 are the ultraviolet (UV) and the infrared (IR) cutoffs in the q integrals. These forms imply that if the q integrals are divergent, the leading terms in $\Sigma^{(2)}(k,\omega)$ must take the form $k^{d+8-\Delta-\delta}\Lambda^\delta$ or $k^{d+8-\Delta+\delta'}m_0^{-\delta'}$, depending on whether the divergences are UV or IR. Here both δ and δ' must be

positive. If the divergences are UV type, we set all internal momentum, such as q and $|\mathbf{k}-\mathbf{q}|$, to Λ, and all internal frequencies to Λ^z. Only external momentum are left intact. Since in $\Sigma^{(2)}(k,\omega)$ the first vertex carries one k^2 and the final vertex carries one external momenta $\mathbf{k}$, the lowest term would be $O(k^2\mathbf{k})$. However, because $\Sigma(k,\omega)$ depends only on k, this term must vanish. Hence, the leading term is $k^4\Lambda^{d+4-\Delta}$. The subleading terms are $k^6\Lambda^{d+2-\Delta}$, $k^8\Lambda^{d-\Delta}$, and so on, with the power of Λ decreasing until the power of Λ becomes negative. For the above to be correct, one requires $\Delta \leq d+4$, and the difference between Δ and $d+4$ decides the number of subleading terms. It is clear that the UV divergences do not contribute any correction to ν_0.

On the other hand, if the divergences are IR type, one sets q or $|\mathbf{k}-\mathbf{q}|$, but not both, to m_0. Simple power counting leads to the conclusion that the leading term of $\Sigma^{(2)}(k,\omega)$ is $k^{6-z}(m_0)^{d+2-\Delta+z}$. The subleading terms are terms with less power of k, so they could correct ν_0. The correction must take the form $k^2(m_0)^{d+6-\Delta}$. Obviously, it implies that $\Delta \geq d+6$, which results in $\chi \geq (6-z)/2 \geq 2$. Since in the physical regime, $\chi \leq 1$ [35], this is also ruled out. Therefore, the IR divergences do not contribute ν_0 in the physical regime ($\chi \leq 1$) either.

Finally, if the integral $\sigma^{(2)}$ is convergent, it depends only on s in the limits $\Lambda \to \infty$ and $m_0 \to 0$. In order that ν_0 gets a correction, we require $\Sigma^{(2)}(k,\omega) \sim k^2$. Hence $d+8-\Delta = 2$, i.e., $\Delta = d+6$. However, this value falls into the regime where the integral $\sigma^{(2)}$ is not convergent, but IR divergent.

The above analysis can be easily generalized to higher-order terms. We find that the dimension of $2n$th order terms in Σ is $n(d+8-\Delta-z)+z$. These terms cannot be both convergent and at the same time contribute $O(k^2)$ because it would imply $\Delta = d+8-2/n+(1/n-1)z$, which is greater than $d+6$ and thus falls into the IR regime. Thus these terms must be divergent. We find that the leading contribution of the UV divergences to Σ are of the form $k^4 \sum_{n=1}^\infty a_n \Lambda^{n(d+6-\Delta)-2}$, where a_n is the contribution of $2n$th order terms; hence the UV divergences do not correct ν_0 at all. Similarly, for IR divergences, possible corrections to ν_0 coming from the $2n$th order terms must be of the form $k^2 m_0^{n(d+8-\Delta-z)+z-2}$. This implies that $\Delta \geq d+8+(1/n-1)z-2/n$, and hence $\chi \geq 4+(1/2n-1)z-1/n \geq 2$, which is not in the physical regime, so the IR divergences do not contribute ν_0 at all in the physical regime ($\chi \leq 1$). We thus conclude that to all orders in the Wyld-Dyson renormalized perturbation expansion, there is no correction to ν_0.

[1] For a recent review, see A.-L. Barabási and H. E. Stanley, *Fractal Concepts in Surface Growth* (Cambridge University Press, Cambridge, 1995).

[2] A. Zangwill, *Physics at Surfaces* (Cambridge University Press, Cambridge, 1988), p. 11.

[3] J. Tersoff, C. Teichert, and M. G. Lagally, Phys. Rev. Lett. **76**, 1675 (1996).

[4] For recent experiments, see Y.-L. He *et al.*, Phys. Rev. Lett. **69**, 3770 (1992); J. Krim *et al.*, *ibid.* **70**, 57 (1993); M. A. Cotta *et al.*, *ibid.* **70**, 4106 (1993).

[5] J. W. P. Hsu *et al.*, Appl. Phys. Lett. **61**, 1293 (1992).

[6] E. A. Fitzgerald *et al.*, J. Vac. Sci. Technol. B **10**, 1807 (1992).

[7] W. T. Pike, R. W. Fathauer, and M. S. Anderson, J. Vac. Sci. Technol. B **10**, 1990 (1992); S. Y. Shiryaev, F. Jensen, and J. W. Petersen, Appl. Phys. Lett. **64**, 3305 (1994); M. A. Lutz *et al.*, *ibid.* **66**, 724 (1995); M. Albrecht, S. Christiansen, J. Michler, W. Dorsch, H. P. Strunk, P. O. Hansson, and E. Bauser, *ibid.* **67**, 1232 (1995); A. G. Cullis, D. J. Robbins, A. J. Pidduck, and P. W. Smith, J. Cryst. Growth **123**, 333 (1992).

[8] Y. Kuramoto, Prog. Theor. Phys. Suppl. **64**, 346 (1978); G. Sivashinsky, Acta Austronautica **4**, 1177 (1977).

[9] F. Family and T. Vicsek, J. Phys. A **18**, L75 (1985).

[10] D. E. Wolf and J. Villain, Europhys. Lett. **13**, 389 (1990).

[11] Z.-W. Lai and S. Das Sarma, Phys. Rev. Lett. **66**, 2348 (1991); S. Das Sarma *et al.*, Phys. Rev. E **53**, 359 (1996).

[12] J. Villain, J. Phys. (France) I **1**, 19 (1991); C. Duport, P. Nozières, and J. Villain, Phys. Rev. Lett. **74**, 134 (1995).

[13] M. Kardar, G. Parisi, and Y.-C. Zhang, Phys. Rev. Lett. **56**, 889 (1986).

[14] The accepted values are $z \sim 1.6$ and $\chi \sim 0.4$; see, e.g., Y. Tu, Phys. Rev. Lett. **73**, 3109 (1994).

[15] For near-equilibrium surfaces, this may be shown to be correct. See C. Herring, *Physics of Powder Metallurgy* (McGraw-Hill, New York, 1951).

[16] This results from simple power counting; see L. H. Tang and T. Nattermann, Phys. Rev. Lett. **66**, 2899 (1991).

[17] M. D. Johnson *et al.*, Phys. Rev. Lett. **72**, 116 (1994); C. Orme *et al.*, Appl. Phys. Lett. **64**, 860 (1994).

[18] V. Yakhot, Phys. Rev. A **24**, 642 (1981).

[19] C. C. Chow and T. Hwa, Physica D **84**, 494 (1995).

[20] V. S. L'vov and I. Procaccia, Phys. Rev. Lett. **69**, 3543 (1992); **72**, 307 (1994); I. Procaccia *et al.*, Phys. Rev. A **46**, 3220 (1992).

[21] C. Jayaprakash, F. Hayot, and R. Pandit, Phys. Rev. Lett. **71**, 12 (1993); **72**, 308 (1994).

[22] C.-Y. Mou and J. W. P. Hsu, Phys. Rev. B **53**, R7610 (1996).

[23] J. Tersoff *et al.*, Phys. Rev. Lett. **75**, 2730 (1995), and references therein.

[24] See, for example, B. J. Spencer, P. W. Voorhees, and S. H. Davis, Phys. Rev. Lett. **67**, 3696 (1991); M. A. Grinfeld, J. Nonlinear Sci. **3**, 35 (1993).

[25] Although *a priori* CVD growth is different from MBE, our CVD chamber was in high vacuum, the growth rate was comparable to MBE, and the sample temperature was kept high. This high vacuum CVD environment is similar to MBE.

[26] E. A. Fitzgerald *et al.*, Appl. Phys. Lett. **59**, 811 (1991): Y. H. Xie *et al.*, J. Mater. Sci. Eng. B **14**, 332 (1992).

[27] Even though the surface features of sample *C* resemble rippling (surface relaxation without dislocations), it is not due to rippling. The ripples on the rippling surfaces are in the $\langle 100 \rangle$ directions. The features on samples *C* are in the $\langle 110 \rangle$ directions, the same directions as the misfit dislocations and the cross-hatch patterns.

[28] M. V. H. Rao, B. K. Mathur, and K. L. Chopra, Appl. Phys. Lett. **65**, 124 (1994).

[29] W. W. Mullins, J. Appl. Phys. **28**, 333 (1957).

[30] S. F. Edwards and D. R. Wilkinson, Proc. R. Soc. London, Ser. A **381**, 17 (1982).

[31] $D_s = D_0 \exp(-E_a/k_b T)$, where D_0, determined by the characteristic phonon frequency and the lattice constant, is of order 10^{-3} cm^2 sec^{-1} and E_a is the activation energy for adatom migration, which is about 0.5 eV [C. Roland and G. H. Gilmer, Phys. Rev. B **47**, 16 286 (1993)].

[32] S. M. Sze, *Physics of Semiconductor Devices* (John Wiley & Sons, New York, 1981).

[33] See, e.g., P. Manneville, *Dissipative Structures and Weak Turbulence* (Academic, New York, 1990).

[34] By large scale, we mean the scales that are larger than the scale of the most unstable modes. In our samples, it means the scales that are larger than the intervalley distances of the cross-hatch patterns.

[35] F. Family and T. Vicsek, *Dynamics of Fractal Surfaces* (World Scientific, Singapore, 1991), pp. 5–40.